Organized Assemblies of Single Wall Carbon Nanotubes and Porphyrin for Photochemical Solar Cells: Charge Injection from Excited Porphyrin into Single-Walled Carbon Nanotubes†

Taku Hasobe,‡,§,|| Shunichi Fukuzumi,*,§ and Prashant V. Kamat*,‡

Radiation Laboratory and Departments of Chemistry & Biochemistry and Chemical & Biomolecular Engineering, University of Notre Dame, Notre Dame, Indiana 46556, and Department of Material and Life Science, Division of Advanced Science and Biotechnology, Graduate School of Engineering, Osaka University, SORST, Japan Science and Technology Agency, Suita, Osaka 565-0871, Japan

Received: July 28, 2006; In Final Form: August 24, 2006

Photochemical solar cells have been constructed from organized assemblies of single-walled carbon nanotubes (SWCNT) and protonated porphyrin on nanostructured SnO_2 electrodes. The protonated form of porphyrin (H_4P^{2+}) and SWCNT composites form 0.5−3.0 μm-sized rodlike structures and they can be assembled onto nanostructured SnO_2 films [optically transparent electrode OTE/SnO_2] by an electrophoretic deposition method. These organized assemblies are photoactive and absorb strongly in the entire visible region. The incident photon to photocurrent efficiency (IPCE) of OTE/SnO_2/SWCNT-H_4P^{2+} is ∼13% at an applied potential of 0.2 V versus saturated calomel electrode. Femtosecond pump−probe spectroscopy experiments confirm the decay of the excited porphyrin in the SWCNT−H_4P^{2+} assembly as it injects electrons into SWCNT. The dual role of SWCNT in promoting photoinduced charge separation and facilitating charge transport is presented.

Introduction

Nanoscale carbon materials (carbon nanotubes and fullerenes) provide new ways to design energy conversion architectures. Construction of molecular electronics and devices based on π-electronic conjugation in cylindrical or spherical structures has already been explored.[1−3] Although solar energy conversion systems using fullerene[4−7] and carbon nanotubes[8] have been explored in recent years, new approaches for production of efficient and low-cost organic solar cells are desired.

Fullerene derivatives that act as electron acceptors have been extensively used in organic solar cells. The electron transfer to C_{60} is highly favored because of the minimal changes in the structure and solvation reorganization following its reduction.[9−13] Bulk heterojunction organic solar cells, which possess an active layer of a conjugated donor polymer and an acceptor fullerene, have been studied extensively.[4−7] Combination of fullerenes with porphyrins yields a supramolecular complex as the fullerene with its 6:6 bond binds to the geometric center of the host porphyrin.[14−17] We have recently demonstrated light energy conversion properties of photovoltaic systems composed of molecular assemblies based on multiporphyrin arrays (porphyrin alkanethiol-protected gold nanoparticles, porphyrin dendrimers, and porphyrin peptide oligomers) and fullerenes deposited on nanostructured SnO_2 electrode [optically transparent electrode OTE/SnO_2].[18] The photoinduced electron transfer between excited porphyrin and C_{60} in these films has been successfully implemented in photoelectrochemical cells. The molecular organization between donor and acceptor moieties was found to be the key factor for the construction of photoelectrochemical cells with improved performance.

Single-walled carbon nanotubes (SWCNT) possess both semiconducting and metallic character. Of particular interest are the optical and electronic properties of semiconducting SWCNT.[19−24] For example, the holes and electrons injected via external circuit produce emission resulting from electron−hole (e−h) recombination in ambipolar carbon nanotube field-effect transistors.[21] The transient absorption and emission measurements demonstrate that the ultrafast relaxation of electrons and holes occurs on a femto- to picosecond time scale (∼100 fs).[22] By making use of the semiconducting property, we have recently investigated photoelectrochemical properties of SWCNT and stacked cup carbon nanotube films.[24] The incident photon-to-photocurrent efficiency (IPCE) in these systems remained low because of rapid exciton annihilation. These initial studies show the ability of carbon nanostructures in promoting charge separation under band gap excitation. New strategies need to be developed to utilize them effectively in a photochemical solar cell.

Surface modification or covalent linkage of molecules often facilitates solubilization of SWCNT, but designing ordered structures of light-harvesting assemblies remains a challenge. The utilization of J- or H-aggregates of porphyrins with acidified medium is a useful approach to form ordered assemblies.[25−29] In a preliminary communication, we have reported formation of ordered assemblies of porphyrins and SWCNT in acidified THF suspension.[30] Both the protonation of the porphyrin and the substituent groups of the porphyrin play an important role in attaining the ordered assemblies.

We report herein photochemical properties of ordered assemblies of protonated porphyrin and SWCNT and their utilization in a photoelectrochemical cell for light-harvesting application. As shown in Scheme 1, the aim is to facilitate charge separation in these assemblies and utilize them to

† Part of the special issue "Arthur J. Nozik Festschrift".

* Corresponding authors: e-mail pkamat@nd.edu (P.V.K.) or fukuzumi@ap.chem.eng.osaka-u.ac.jp (S.F.).

‡ University of Notre Dame.

§ Osaka University.

|| Present address: School of Materials Science, Japan Advanced Institute of Science and Technology, Nomi, Ishikawa, 923-1292, Japan.

10.1021/jp064845u CCC: $33.50
Published on Web 09/29/2006

SCHEME 1: Photoinduced Charge Injection from Excited Porphyrin into SWCNT

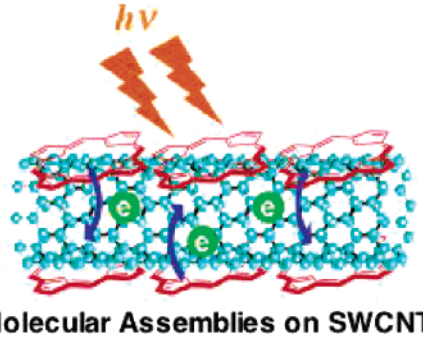

generate photocurrent by suitable manipulation in a photoelectrochemical cell. To probe the role of substituents in forming ordered assemblies, we have also employed three porphyrin derivatives, [5,15-bis(3,5-di-*tert*-butylphenyl)porphyrin (H_2P), 5,10,15,20-tetra(3,5-di-*tert*-butylphenyl)porphyrin (H_2PTBuP), and 5,10,15,20-tetraphenylporphyrin (H_2PTTP)] (Figure 1).

Experimental Section

General. Melting points were recorded on a Yanagimoto micro-melting point apparatus and were not corrected. ^1H NMR spectra were measured on a JEOL EX-270 (270 MHz) or a JEOL JMN-AL300 (300 MHz). Matrix-assisted laser desorption/ionization (MALDI) time-of-flight (TOF) mass spectra were measured on a Kratos Compact MALDI I (Shimadzu). UV−visible spectra were recorded on a Shimadzu 3101 spectrophotometer. Transmission electron micrograph (TEM) measurements were recorded by applying a drop of the sample to a carbon-coated copper grid. Images were recorded on a Hitachi H600 transmission electron microscope. The morphology of the mesoporous electrodes was characterized by a scanning electron micrograph (SEM; JEOL, JSM-6700F).

Materials. All solvents and chemicals were of reagent-grade quality, obtained commercially and used without further purification unless otherwise noted (vide infra). The synthesis of H_2P and H_2PTBuP has been reported elsewhere.[31] H_2PTPP was purchased from Sigma Aldrich Co. Protonated formations of H_2P, H_2PTBuP, and H_2PTPP are referred as H_4P^{2+}, H_4PTBuP^{2+}, and H_4PTPP^{2+}, respectively. The purification procedure of SWCNT (Nanocs Inc.) was adapted from the reported procedure.[32] Thin-layer chromatography (TLC) and flash column chromatography were performed with 5554 DC−Alufolien Kieselgel 60 F_{254} (Merck), and Fujisilicia BW300, respectively. Nanostructured SnO_2 films were cast on an optically transparent electrode (OTE) by applying a 2% colloidal solution obtained from Alfa Chemicals. The air-dried films were annealed at 673 K. The details of the preparation of SnO_2 films on conducting glass substrate were reported elsewhere.[33] The nanostructured SnO_2 film electrode is referred as OTE/SnO_2.

Electrophoretic Deposition of Cluster Films. A known amount of porphyrin derivatives, C_{60}, or mixed cluster solution in acetonitrile/toluene (3/1 v/v, 2 mL) was transferred to a 1 cm cuvette in which two electrodes (viz., OTE/SnO_2 and OTE) were kept at a distance of 6 mm by use of a Teflon spacer. A dc voltage (200 V) for 2 min was applied between these two electrodes by use of a Fluke 415 power supply. The deposition of the film can be visibly seen as the solution becomes colorless with simultaneous brown coloration of the OTE/SnO_2 electrode. The OTE/SnO_2 electrode coated with molecular assemblies of SWCNT and porphyrin is referred to as OTE/SnO_2/SWCNT−porphyrin.

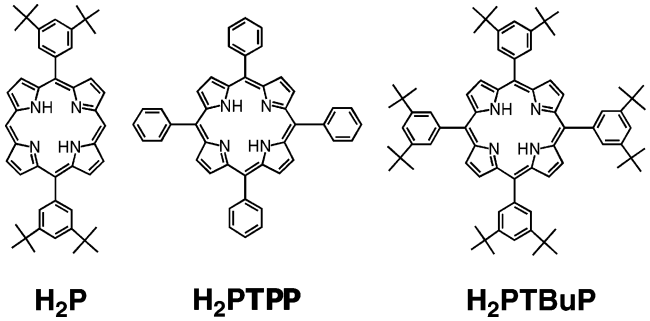

Figure 1. Structures of porphyrin derivatives.

Photoelectrochemical Measurements. Photoelectrochemical measurements were carried out in a standard three-compartment cell consisting of a working electrode, a Pt wire gauze counterelectrode, and a saturated calomel reference electrode (SCE). This configuration allowed us to carry out photocurrent measurements under electrochemical bias. A Princeton Applied Research (PAR) model 173 potentiostat and model 175 universal programmer were used for recording I−V characteristics. All other photoelectrochemical measurements were carried out with a Pt gauge counterelectrode in the same cell assembly by use of a Keithley model 617 programmable electrometer. The electrolyte was 0.5 M NaI and 0.01 M I_2 in acetonitrile. A collimated light beam from a 150 W xenon lamp with a 400 nm cutoff filter was used for excitation of porphyrin−SWCNT films cast on SnO_2 electrodes. A Bausch and Lomb high-intensity grating monochromator was introduced into the path of the excitation beam for the selected wavelength.

Femtosecond Time-Resolved Laser Flash Photolysis. Ultrafast transient absorption spectroscopy experiments were conducted with a Clark-MXR 2010 laser system and an optical detection system provided by Ultrafast Systems (Helios). The source for the pump and probe pulses were derived from the fundamental output of Clark laser system (775 nm, 1 mJ/pulse and fwhm = 150 fs) at a repetition rate of 1 kHz. A second harmonic generator introduced in the path of the laser beam provided 387 nm laser pulses for excitation. Of the fundamental output of the laser (775 nm), 95% was used to generate the second harmonic, while 5% of the deflected output was used for white light generation. Prior to generation of the probe continuum, the laser pulse was fed to a delay line that provided an experimental time window of 1.6 ns with a maximum step resolution of 7 fs. The pump beam was attenuated at 5 μJ/pulse with a spot size of 2 mm diameter at the sample cell where it was merged with the white probe pulse in a close angle (<10°). The probe beam, after passing through the 2 mm sample cell, was focused on a 200 μm fiber optic cable that was connected to a CCD spectrograph (Ocean Optics, S2000−UV−vis) for recording the time-resolved spectra (425−800 nm). Typically, 5000 excitation pulses were averaged to obtain the transient spectrum at a set delay time. Kinetic traces at appropriate wavelengths were assembled from the time-resolved spectral data. All measurements were conducted at room temperature, 295 K. When necessary, a flow cell was used to circulate the solution through the sample cell.

Results and Discussion

Interaction of Protonated Porphyrin and SWCNT and Formation of Ordered Assemblies. $\pi-\pi$ interaction between protonated porphyrin and SWCNT facilitates ordered structuring of composite assemblies. As shown in our preliminary communication, SWCNT serves as a template to achieve ordered

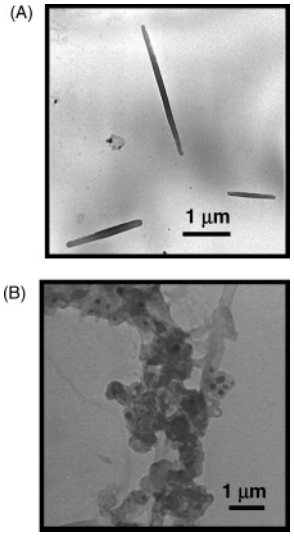

Figure 2. Transmission electron micrograph (TEM) images of SWCNT−porphyrin assemblies obtained in acidified THF: (A) SWCNT−H_4P^{2+} (ref 30) and (B) SWCNT−H_4PTPP^{2+}

structures.[30] The assembly of SWCNT-protonated porphyrin was obtained by the following procedure. Purified SWCNT (1 mg) were added to a 0.2 mM solution of porphyrin in tetrahydrofuran (THF) containing 1.0% H_2SO_4 (v/v). The suspension was sonicated for 1 h at room temperature, followed by centrifugation of the suspension for 30 min at 10 000 rpm to separate the SWCNT-protonated porphyrin composite. The solid was resuspended in acidified THF with sonication (1 h) and centrifuged again to wash out any unbound porphyrin. The solid was resuspended in acidified THF. The suspension of SWCNT-protonated porphyrin was stable for carrying out microscopy and spectroscopy measurements.

Figure 2 shows the ordered assemblies obtained with protonated and unprotonated forms of porphyrin and SWCNT in THF solution. The rodlike structures show that interaction between H_4P^{2+} and SWCNT produces ordered assemblies. (Figure 2A). In the absence of an acidic medium, the unprotonated porphyrin fails to yield such an ordered structure. Isolated H_2P clusters were formed as the interaction between H_2P and SWCNT remains weak in neat THF.[30] Substituent groups also influenced the interaction with SWCNT and overall assembly of ordered structures. H_4PTBuP^{2+} failed to bind to the SWCNT surface in THF suspension. Efforts to extract molecular assemblies after centrifugation did not yield SWCNT−H_4PTBuP^{2+} composite. Almost all H_4PTBuP^{2+} remained in the solution phase. Large steric hindrance from 3,5-di-*tert*-butylphenyl groups at four meso positions in H_2PTBuP is likely to weaken the interaction with SWCNT. In the case of SWCNT−H_4PTPP^{2+}, the interaction with SWCNT results in the formation of 200−300 nm diameter clusters. These clusters can be extracted after the centrifugation procedure. The interaction of H_4PTPP^{2+} with SWCNT was not strong enough to produce rodlike ordered assemblies. These TEM images show the importance of substituent groups of the porphyrin moiety in controlling the interaction with SWCNT and ordering of these composites through inter- and intramolecular interatcions.

Figure 3 shows the absorption spectra recorded after sonication of H_4P^{2+}, H_4PTBuP^{2+}, and H_4PTPP^{2+} in acidified THF suspension containing SWCNT and redispersion of centrifugate in acidified THF. This procedure allowed us to characterize the spectral features of porphyrin−SWCNT composites. The spectral differences indicate that the molecular assemblies of porphyrins on the SWCNT surface largely depend on the

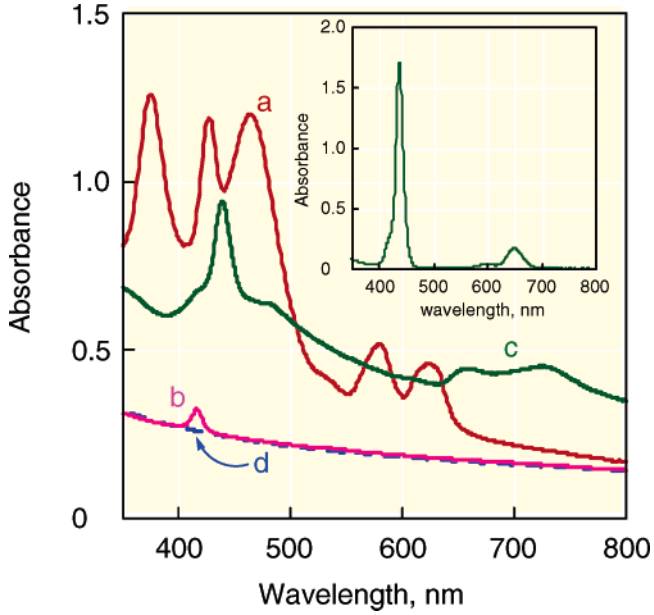

Figure 3. Absorption spectra of (a) SWCNT−H_4P^{2+}, (b) SWCNT−H_4PTBuP^{2+}, (c) SWCNT−H_4PTPP^{2+} and (d) SWCNT in acidified THF after the centrifugation and redispersion procedures. The concentration of protonated porphyrins was 0.2 mM. (Inset) Monomeric form of H_4PTPP^{2+} (0.01 mM) in acidified THF.

substituents in a porphyrin ring. Only samples containing H_4P^{2+} and H_4PTPP^{2+} yielded noticeable absorption after redispersion of the centrifugate, thus confirming the association with SWCNT. The absence of noticeable absorption confirms that H_4PTBuP^{2+} does not interact with the SWCNT surface effectively.

Of particular interest is the interaction between SWCNT and H_4P^{2+}, which produced ordered assemblies. Formation of such ordered assemblies is characterized by the aggregation of porphyrin.[30] The protonated form of the porphyrin in acidified THF shows a Soret band at 427 nm. Two sharp peaks (375 and 460 nm) in addition to the parent Soret band, corresponding to J- and H-aggregates, could be seen in absorption spectrum a in Figure 3. H_2PTPP, with less bulky phenyl groups at four meso positions in the porphyrin ring, interacts with SWCNT in acidified THF but fails to show ordered structures. The Soret band exhibits little change in the SWCNT−H_4PTPP^{2+} composite form. Interestingly, the spectrum of SWCNT−H_4PTPP^{2+} becomes very broad in the near-infrared region. The maximum peak at 651 nm in the monomeric form becomes broad and red-shifted to 722 nm in SWCNT−H_4PTPP^{2+} as a result of interactions within the composite. In contrast, the interaction between SWCNT−H_4PTBuP^{2+} is considered negligible. These results, based on molecular assemblies of SWCNT with three types of porphyrins with different substituent groups at meso positions, show that structural control of dye moieties is essential for construction of supramolecular assemblies with SWCNT. Both TEM and absorption spectroscopy confirm the formation of ordered assemblies between H_4P^{2+} and SWCNT.

Deposition of SWCNT-Porphyrins Composites on OTE/SnO_2 Film. The highly colored composite molecular assemblies of SWCNT−H_4P^{2+} were assembled as three-dimensional arrays onto a nanostructured SnO_2 electrode. The electrophoretic deposition procedure described earlier[24,34] was followed to deposit SWCNT−porphyrin composites from a THF suspension. Upon application of a dc electric field of 200 V for 2 min between the OTE/SnO_2 and OTE electrodes, which were kept parallel in THF suspension containing SWCNT−porphyrin, the

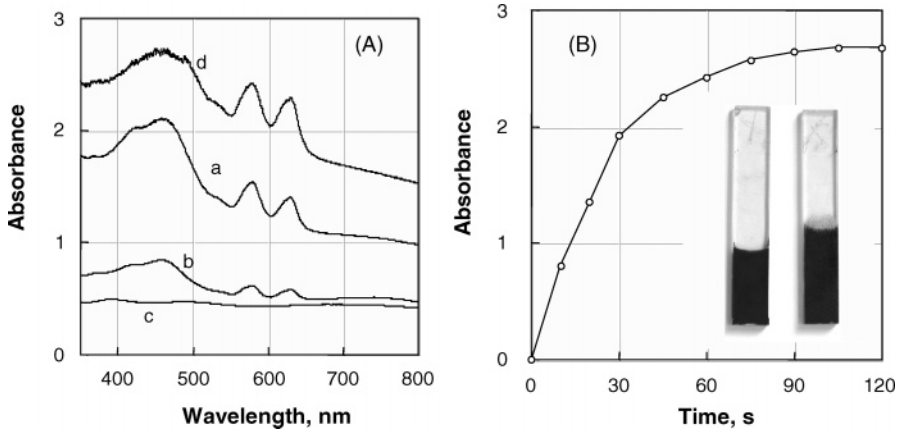

Figure 4. (A) Absorption spectra of (a) OTE/SnO_2/SWCNT−H_4P^{2+} film, (b) OTE/SnO_2/H_4P^{2+} film, and (c) OTE/SnO_2/SWCNT film. [H_4P^{2+}] = 0.2 mM, SWCNT 1 mg. (d) Same as trace (a) but with [H_4P^{2+}] = 0.4 mM. (B) Absorption change at 460 nm of OTE/SnO_2/SWCNT−H_4P^{2+} electrode at different time intervals during electrophoretic deposition process. ([H_4P^{2+}] = 0.2 mM, SWCNT 1 mg). (Inset) Image of the electrode after deposition of the SWCNT−H_4P^{2+} assembly.

composite assmblies are deposited on the SnO_2 nanocrystallites. As the deposition continues, the suspension loses color with simultaneous coloration of the electrode. Figure 4B shows the absorption changes of the OTE/SnO_2 electrode observed with duration of electrophoresis. Increased absorbance of the electrode confirms the deposition of the SWCNT−H_4P^{2+} as a film. (The electrode will be referred to as OTE/SnO_2/SWCNT−H_4P^{2+}).

Absorption spectra of electrodes prepared from THF suspensions of SWCNT−H_4P^{2+}, H_4P^{2+}, and SWCNT are shown in Figure 4A. The spectrum of OTE/SnO_2/SWCNT−H_4P^{2+} (spectrum a) shows strong absorption in the visible and near-IR regions. The SWCNT film exhibits featureless absorption (spectrum c). The absorption arising from porphyrin (spectrum b) in OTE/SnO_2/H_4P^{2+} is further reflected in the spectrum of OTE/SnO_2/SWCNT (spectrum a). These results ensure that incident light is absorbed effectively in the visible and near-IR regions by OTE/SnO_2/SWCNT−H_4P^{2+}. The three sharp absorption peaks in the Soret band region of SWCNT−H_4P^{2+} observed in THF suspension appear as a broad absorption in OTE/SnO_2/SWCNT−H_4P^{2+} electrode. It is likely that the strong aggregation and intermolecular interaction of H_4P^{2+} moieties induce broadening of the absorption band. We also prepared electrodes from SWCNT−H_4PTPP^{2+} composite. The spectrum of OTE/SnO_2/SWCNT−H_4PTPP^{2+} exhibited broad absorption in the visible region and found to be similar to that of OTE/SnO_2/SWCNT-H_4P^{2+} electrode.

We also characterized the SWCNT−porphyrin composite film electrodes by scanning electron microscopy (SEM). The SEM images of OTE/SnO_2/SWCNT−H_4P^{2+}, OTE/SnO_2/H_4P^{2+}, and OTE/SnO_2/SWCNT are displayed in Figure 5. The molecular assembly of OTE/SnO_2/SWCNT−H_4P^{2+} (Figure 5A) is different than those of single-component systems (panels B and C in Figure 5: OTE/SnO_2/H_4P^{2+} and OTE/SnO_2/SWCNT, respectively). The assembly of 100−200 nm size clusters of various shapes is observed in OTE/SnO_2/H_4P^{2+}. SWCNT assembled in OTE/SnO_2/SWCNT film usually consist of bundles of carbon nanotubes.

Photodynamics of Molecular Assemblies of SWCNT−H_4P^{2+}. To investigate the light-harvesting properties of SWCNT−H_4P^{2+} composite, we probed the photoinduced transformation using femtosecond pump−probe spectroscopy. In our previous study,[30] we reported quenching of porphyrin fluorescence upon its interaction with SWCNT. The steady-state fluorescence of SWCNT−H_4P^{2+} composite in THF suspension was significantly

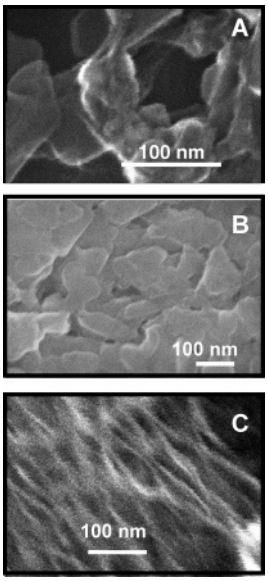

Figure 5. SEM images of (A) OTE/SnO_2/SWCNT−H_4P^{2+} film ([H_4P^{2+}] = 0.2 mM, SWCNT 1 mg), (B) OTE/SnO_2/H_4P^{2+} film ([H_4P^{2+}] = 0.2 mM), and (C) electrophoretically deposited SWCNT film (ref 33c).

lower than that of H_4P^{2+} alone. The excited-state quenching of H_4P^{2+} indicates that SWCNT assisted deactivation of the singlet excited state. Similar quenching of porphyrin emission by SWCNT has been noted in earlier studies.[30,35] It is proposed that the deactivation of the excited chromophore involves charge transfer to SWCNT.

The response of SWCNT to laser pulse excitation has also been noted in earlier studies.[36−39] The photoinduced transformations involving exciton generation and charge separation are completed within the 130 fs laser pulse duration and can be followed from the bleaching in the visible region.[36] The broad band of bleaching essentially depends on the diversity of tube diameters, chiral angle, and aggregation of nanotubes. The bleaching in the visible region, which corresponds to the C_2-V_2 transition, recovers in ~1 ps as the bound e−h pairs or excitons are relaxed to the low-lying C_1-V_1 state. The e−h pairs that accumulate in the fundamental gap (C_1-V_1) quickly decay within few picoseconds.[36c] In the present study, most of the excitation is centered around the porphyrin moiety and the contribution from the SWCNT to the transient absorption measurements is considered negligible.

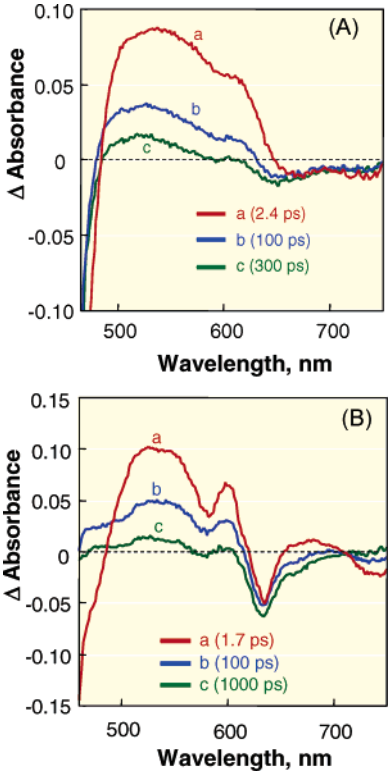

Figure 6. Time-resolved absorption spectra of (A) SWCNT−H_4P^{2+} in THF ([H_4P^{2+}] = 0.2 mM) and (B) H_4P^{2+} in THF ([H_4P^{2+}] = 0.2 mM). Excitation wavelength is 387 nm.

Figure 6 panels A and B show time-resolved transient absorption spectra recorded following 387 nm laser pulse excitation of SWCNT−H_4P^{2+} and H_4P^{2+} in THF suspension, respectively. In the case of H_4P^{2+}, the characteristic broad absorption of singlet excited state in the 480−600 nm region appears immediately after laser pulse excitation (Figure 6B). As the singlet excited state decays, one observes formation of the triplet excited state. The residual absorption seen at longer times is characteristic of the triplet excited porphyrin. The negative absorbance seen in the red region essentially arises from the porphyrin fluorescence and this emission cannot be time-resolved in our femtosecond detection system. It is interesting to note that the signal arising from the porphyrin fluorescence is absent in the case of SWCNT−H_4P^{2+} composite, further confirming the excited-state interaction with SWCNT. Comparison of the spectral features in Figure 6 panels A and B shows the formation of additional transient species in the SWCNT−H_4P^{2+} system.

To further establish these differences, we have compared the absorption−time profiles of SWCNT−H_4P^{2+} with those of H_4P^{2+} at 525, 470, and 625 nm in Figure 7. Rapid quenching of the excited porphyrin in SWCNT−H_4P^{2+} was evident from the decay comparison at 525 nm. The time profile at 470 nm for H_4P^{2+} shows sustained bleaching arising from the formation of triplet excited state. The lack of such bleaching in the case of SWCNT−H_4P^{2+} shows the absence of intersystem crossing during the deactivation of the singlet excited porphyrin. These two sets of decay traces further confirm that SWCNT is able to interact directly with the singlet excited porphyrin aggregates. If indeed such excited-state quenching of porphyrin by SWCNT should involve a charge-transfer process, we should be able to characterize the products of the reaction, viz., porphyrin cation radical. The absorption−time profile of H_4P^{2+} alone at 625 nm is dominated by the fluorescence emission. However, we can observe the formation of radical cation from the positive

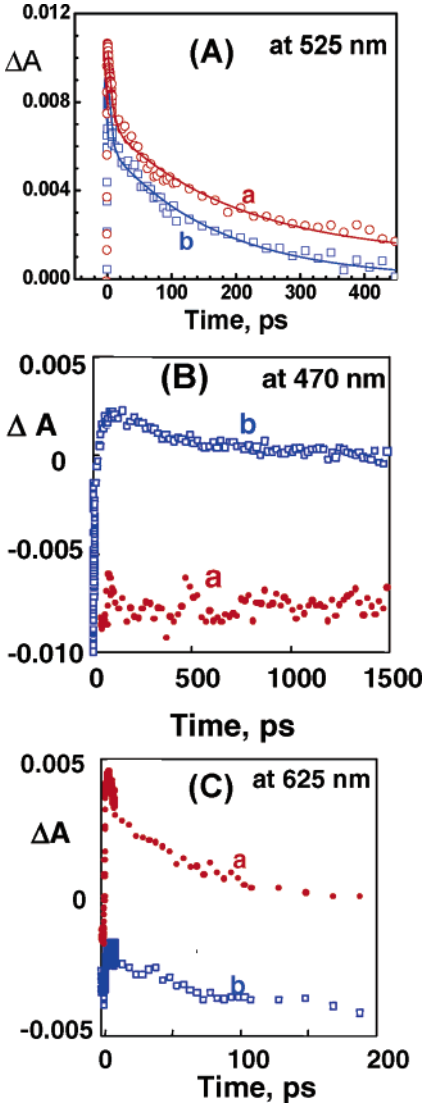

Figure 7. Absorption−time profiles recorded at (A) 525 nm, (B) 470 nm, and (C) 625 nm following the 387 nm (130 fs pulse width) laser pulse excitation of H_4P^{2+} in THF: (a) in the absence and (b) in the presence of SWCNT.

absorbance of trace b in Figure 7C. The radical cation species of free base porphyrin are typically observed in this region.[18,40] A residual absorbance is retained even at the end of 1 ns, thus confirming the long-lived charge separation. On the basis of these results, we can conclude that photoinduced electron-transfer quenching occurs from the singlet excited state of H_4P^{2+} to SWCNT after irradiation in the composite molecular assemblies of SWCNT−H_4P^{2+}. As shown earlier,[22] the conduction band of semiconducting SWCNT is in the range of 0−0.5 V versus NHE. Such energetics of the SWCNT favor charge injection from excited porphyrin into SWCNT bundles:

$$\text{SWCNT}-(H_4P^{2+}) + h\nu \rightarrow \text{SWCNT}-{}^1(H_4P^{2+})^* \quad (1)$$

$$\text{SWCNT}-{}^1(H_4P^{2+})^* \rightarrow \text{SWCNT(e)} - (H_4P^{3+}) \quad (2)$$

Photoelectrochemical Properties of OTE/SnO_2 Electrode. To evaluate the photoelectrochemical performance of the SWCNT−H_4P^{2+} films, we used OTE/SnO_2/SWCNT−H_4P^{2+} as a photoanode in a photoelectrochemical cell (Scheme 2).

Photocurrent measurements were performed in acetonitrile containing NaI (0.5 M) and I_2 (0.01 M) as redox electrolyte

SCHEME 2: Photoelectrochemical Cell Based on SWCNT−Porphyrin Light-Harvesting Assembly

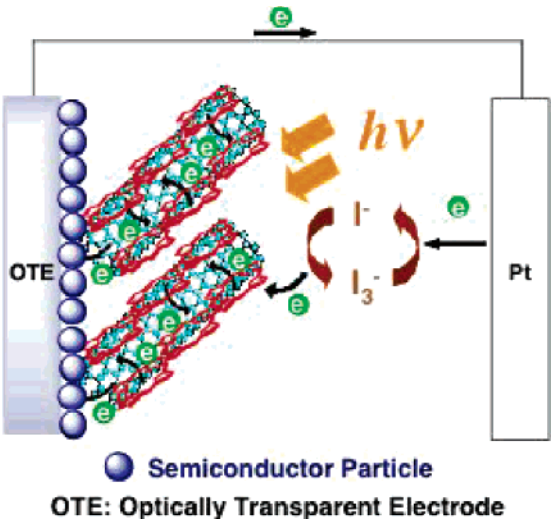

with a Pt gauge counterelectrode. The photovoltage and photocurrent responses upon the excitation of OTE/SnO_2/SWCNT−H_4P^{2+} electrode in the visible region (λ > 400 nm) are shown in Figure 8, panels A and B, respectively. The photocurrent response is prompt, steady, and reproducible during repeated on/off cycles of the visible light illumination. The short circuit photocurrent density (I_{sc}) is 0.10 mA/cm^2, and open circuit voltage (V_{oc}) is 60 mV; these values were reproducibly obtained during visible excitation (input power 12.4 mW cm^{-2}). We have also measured the power conversion efficiency (η) of the photoelectrochemical cell by varying the load resistance. A fill factor of 0.24 and overall power conversion efficiency of 0.012% at input power (W_{in}) of 12.4 mW cm^{-2} were obtained for the photoelectrochemical cell employing OTE/SnO_2/SWCNT-H_4P^{2+} electrode.

Blank experiments conducted with OTE/SnO_2 [i.e., by excluding composite molecular assemblies (SWCNT−H_4P^{2+})] produced no detectable photocurrent under similar experimental conditions. These experiments confirmed the charge-transfer interaction in the SWCNT−H_4P^{2+} assembly can be beneficially used to generate photocurrent.

The charge separation in the OTE/SnO_2/SWCNT−H_4P^{2+} electrode assembly can be further modulated by the application of an electrochemical bias. Figure 8C shows current−voltage ($I-V$) characteristics of the OTE/SnO_2/SWCNT−H_4P^{2+} electrode under visible light illumination. The photocurrent increases as the applied potential is scanned toward positive potentials. Increased charge separation and the facile transport of charge carriers under positive bias contribute to the enhanced photocurrent generation. At potentials greater than +0.3 V versus SCE, direct electrochemical oxidation of iodide interferes with the photocurrent measurement.[41]

Photocurrent Action Spectra of OTE/SnO_2 Electrode. If photoinduced electron transfer in SWCNT−H_4P^{2+} composite is responsible for the photocurrent generation, we should be able to further resolve the origin of the effect by recording photocurrent action spectra (Figure 9). The IPCE (incident photon-to-photocurrent efficiency) values were calculated by normalizing the photocurrent values for incident light energy and intensity by use of eq 3:[18]

$$\text{IPCE (\%)} = 100 \times 1240 \times I_{sc}/(I_{inc} \times \lambda) \qquad (3)$$

where I_{sc} is the short circuit photocurrent (amps per square centimeter), I_{inc} is the incident light intensity (watts per square centimeter), and λ is the wavelength (nanometers). The IPCE spectra obtained from the photocurrent measurements in the absence of applied bias are shown in Figure 9A. The broad photocurrent response of OTE/SnO_2/SWCNT−H_4P^{2+} (spectrum a) in the visible region matches the absorption features recorded in Figure 4. The maximum IPCE value (∼6.5%) obtained for OTE/SnO_2/SWCNT−H_4P^{2+} is greater than those obtained for the individual components, viz., OTE/SnO_2/SWCNT (∼0.1%; spectrum c) and OTE/SnO_2/H_4P^{2+} (∼1.5%; spectrum b).[42] These results indicate that the photoinduced charge separation in the composite molecular assemblies of SWCNT−-H_4P^{2+} plays an important role in the photocurrent generation. In comparison, the maximum IPCE value of OTE/SnO_2/SWCNT−H_4PTPP^{2+} is ∼3.0% (spectrum d). Lower IPCE observed for OTE/SnO_2/SWCNT−H_4PTPP^{2+} is attributed to the fact that H_4PTPP^{2+} produces poorly organized molecular assemblies.

By controlling the potential of OTE/SnO_2 with an electrochemical bias, we can improve the charge separation and attain higher IPCE values. The photocurrent action spectra of OTE/SnO_2/SWCNT−H_4P^{2+}) under applied bias potentials of 0.1 and 0.2 V versus SCE were recorded with a standard three-compartment cell as a working electrode along with Pt wire

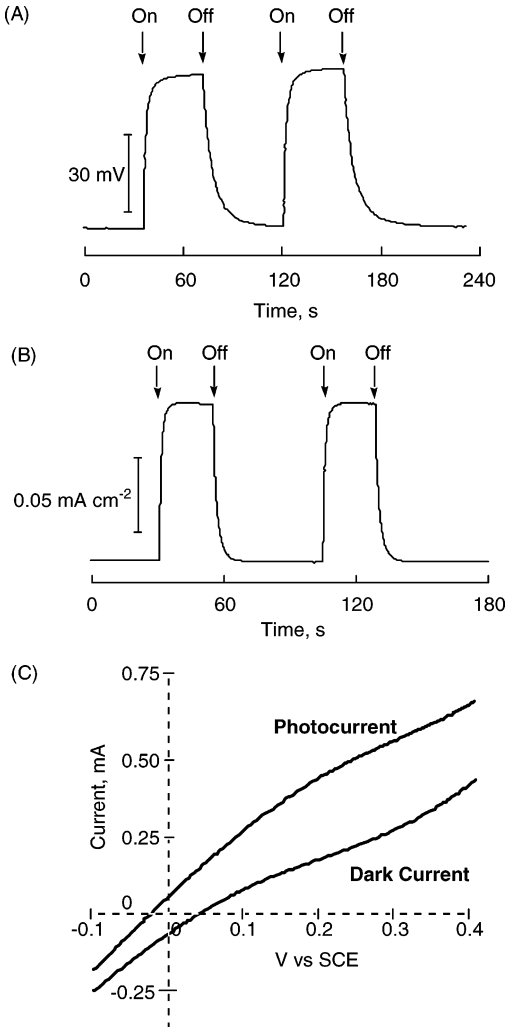

Figure 8. (A) Photovoltage and (B) photocurrent responses of OTE/SnO_2/SWCNT−H_4P^{2+} electrode ([H_4P^{2+}] = 0.2 mM, SWCNT 1 mg) under white light illumination. (C) $I-V$ characteristics of OTE/SnO_2/SWCNT−H_4P^{2+} electrode ([H_4P^{2+}] = 0.2 mM, SWCNT 1 mg) under white light illumination (λ > 400 nm). Electrolyte: NaI 0.5 M, I_2 0.01 M in acetonitrile; input power = 12.4 mW cm^{-2}.

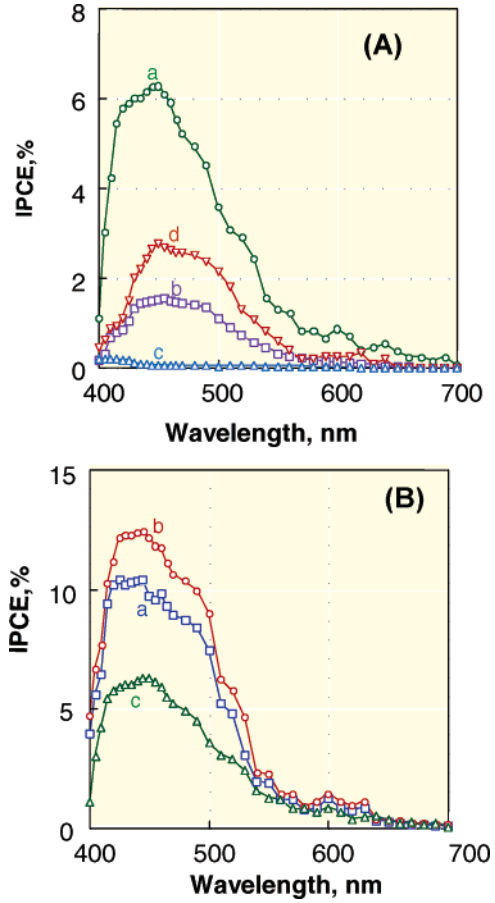

Figure 9. (A) Photocurrent action spectra of (a) OTE/SnO_2/SWCNT−H_4P^{2+} electrode ([H_4P^{2+}] = 0.2 mM, SWCNT 1 mg), (b) OTE/SnO_2/H_4P^{2+} electrode ([H_4P^{2+}] = 0.2 mM), (c) OTE/SnO_2/SWCNT electrode, and (d) OTE/SnO_2/SWCNT−H_4PTPP^{2+} electrode ([H_4PTPP^{2+}] = 0.2 mM, SWCNT 1 mg) with no applied bias potential. (B) Photocurrent action spectra of OTE/SnO_2/SWCNT−H_4P^{2+} electrode ([H_4P^{2+}] = 0.2 mM, SWCNT 1 mg) at an applied bias potential of (a) 0.1 V vs SCE or (b) 0.2 V vs SCE, or (c) with no applied bias potential. Electrolyte: NaI 0.5 M, I_2 0.01 M in acetonitrile.

gauze counterelectrode and saturated calomel reference electrode (SCE) (spectra a and b in Figure 9B, respectively).[43] The maximum IPCE values of OTE/SnO_2/SWCNT−H_4P^{2+}) under applied bias potentials of 0.1 and 0.2 V versus SCE were 10% and 13%, respectively. These values are an order of magnitude greater than the one observed for CdS−SWCNT composite film.[44] On the basis of these photoelectrochemical experiments, we can conclude that organization of molecular assemblies achieved with SWCNT−H_4P^{2+} is a key factor in attaining improved light energy conversion properties.

The photocurrent generation efficiency observed with OTE/SnO_2/SWCNT−H_4P^{2+} is greater than those observed with the individual systems (viz., OTE/SnO_2/SWCNT and OTE/SnO_2/H_4P^{2+}). As illustrated in the transient absorption measurements, photoinduced charge injection from the singlet excited state of porphyrin into SWCNT is the primary event responsible for the photocurrent generation. While the electrons are transported across the carbon nanotube network to the collecting electrode, the oxidized porphyrin undergoes electron transfer with iodide−triiodide redox couple and regenerates the sensitizer. Thus, the SWCNT provides the dual role of promoting charge transfer by interacting with excited porphyrin and serving as conduit to transport the injected electron to the collecting electrode. Careful design of such nanotube architectures may provide the basis for improving the performance of photochemical solar cells.[44,45] Recently, polymer solar cells based on poly(3-hexylthiophene) and methanofullerene have shown efficiencies as high as 4.4%.[45c] The presence of methanofullerene facilitates charge separation and transport in the active layer. The results presented in this study show the usefulness of carbon nanotubes in building organized solar cells.

Conclusions

We have succeeded in the construction of a photoelectrochemical solar cell with a light-harvesting nanoarchitecture consisting of carbon nanotubes and porphyrin moieties. Molecular assemblies of protonated porphyrin and SWCNT were assembled as three-dimensional arrays onto nanostructured SnO_2 films by an electrophoretic deposition method. The composite cluster electrode of SWCNT−H_4P^{2+} exhibits an incident photon-to-photocurrent efficiency (IPCE) as high as 13% under an applied potential of 0.2 V versus SCE. Femtosecond transient absorption studies confirm photoinduced electron transfer between excited H_4P^{2+} and SWCNT. The photoelectrochemical effect observed with SWCNT and porphyrin assembly demonstrates the usefulness of carbon nanotubes in promoting charge transfer and charge transport in photochemical solar cells.

Acknowledgment. This work was partially supported by Grant-in-Aids for Scientific Research (16205020 to S.F.) and for COE Research (Osaka University, Integrated Ecochemistry) from the Ministry of Education, Culture, Sports, Science and Technology, Japan. P.V.K. acknowledges support from the Office of Basic Energy Science of the U.S. Department of the Energy. This is Contribution NDRL 4879 from the Notre Dame Radiation Laboratory and from Osaka University.

Supporting Information Available: Current−voltage (*I*−*V*) characteristics of OTE/SnO_2/SWCNT electrode under no photoexcitation (Figure S1), photocurrent action spectrum of OTE/SnO_2/SWCNT−H_4P^{2+} prepared from the suspension with high concentration of H_4P^{2+} (Figure S2), the absorption spectrum (Figure S3), and the estimation of power conversion efficiency of OTE/SnO_2/SWCNT−H_4P^{2+} (Figure S4). This material is available free of charge via the Internet at http://pubs.acs.org.

References and Notes

(1) (a) Niyogi, S.; Hamon, M. A.; Hu, H.; Zhao, B.; Bhomwik, P.; Sen, R.; Itkis, M. E.; Haddon, R. C. *Acc. Chem. Res.* **2002**, *35*, 1105. (b) Hirsch, A. *Angew. Chem., Int. Ed.* **2002**, *41*, 1853. (c) Sun, Y.-P.; Fu, K.; Lin, Y.; Huang, W. *Acc. Chem. Res.* **2002**, *35*, 1096. (d) Guldi, D. M.; Rahman, G. M. A.; Zerbetto, F.; Prato, M. *Acc. Chem. Res.* **2005**, *38*, 871. (e) Weisman, R. B.; Subramoney, S. *Interface* **2006**, *15*, 42.

(2) (a) Bahr, J. L.; Tour, J. M. *J. Mater. Chem.* **2002**, *12*, 1952. (b) Banerjee, S.; Kahn, M. G. C.; Wang, S. S. *Chem.—Eur. J.* **2003**, *9*, 1898. (c) Dyke, C. A.; Tour, J. M. *Chem.—Eur. J.* **2004**, *10*, 812. (d) Tasis, D.; Tagmatarchis, N.; Georgakilas, V.; Prato, M. *Chem.—Eur. J.* **2003**, *9*, 4000. (e) Giacalone, F.; Segura, J. L.; Martin, N.; Ramey, J.; Guldi, D. M. *Chem.—*Eur. J. **2005**, *11*, 4819. (f) Giacalone, F.; Segura, J. L.; Martin, N.; Guldi, D. M. *J. Am. Chem. Soc.* **2004**, *126*, 5340.

(3) (a) Yu, L. H.; Natelson, D. *Nano Lett.* **2004**, *4*, 79. (b) Park, H.; Park, J.; Lim, A. K. L.; Anderson, E. H.; Alivisatos, A. P.; McEuen, P. L. *Nature* **2000**, *407*, 57. (c) Freitag, M.; Perebeinos, V.; Chen, J.; Stein, A.; Tsang, J. C.; Misewich, J. A.; Martel, R.; Avouris, P. *Nano Lett.* **2004**, *4*, 1063.

(4) (a) Yu, G.; Gao, J.; Hummelen, J. C.; Wudl, F.; Heeger, A. J. *Science* **1995**, *270*, 1789−1791. (b) Wudl, F. *J. Mater. Chem.* **2002**, *12*, 1959−1963.

(5) (a) Shaheen, S. E.; Brabec, C. J.; Sariciftci, N. S.; Padinger, F.; Fromherz, T.; Hummelen, J. C. *Appl. Phys. Lett.* **2001**, *78*, 841−843. (b) Padinger, F.; Rittberger, R. S.; Sariciftci, N. S. *Adv. Funct. Mater.* **2003**, *13*, 85−88.

(6) (a) Schmidt-Mende, L.; Fechtenkötter, A.; Müllen, K.; Moons, E.; Friend, R. H.; MacKenzie, J. D. *Science* **2001**, *293*, 1119−1122. (b) Halls, J. J. M.; Walsh, C. A.; Greenham, N. C.; Marseglia, E. A.; Friend, R. H.;

Moratti, S. C.; Holmes, A. B. *Nature* **1995**, *376*, 498−500. (c) Zerza, G.; Scharber, M. C.; Brabec, C. J.; Sariciftci, N. S.; Gomez, R.; Segura, J. L.; Martin, N.; Srdanov, V. I. *J. Phys. Chem. A* **2000**, *104*, 8315, (d) Hoppe, H.; Sariciftci, N. S. *J. Mater. Res.* **2004**, *19*, 1924.

(7) (a) Wienk, M. M.; Kroon, J. M.; Verhees, W. J. H.; Knol, J.; Hummelen, J. C.; van Hal, P. A.; Janssen, R. A. J. *Angew. Chem., Int. Ed.* **2003**, *42*, 3371−3375. (b) Dhanabalan, A.; van Duren, J. K. J.; van Hal, P. A.; van Dongen, J. L. J.; Janssen, R. A. J. *Adv. Funct. Mater.* **2001**, *11*, 255−262. (c) Eckert, J.-F.; Nicoud, J.-F.; Nierengarten, J.-F.; Liu, S.-G.; Echegoyen, L.; Barigelletti, F.; Armaroli, N.; Ouali, L.; Krasnikov, V.; Hadziioannou, G. *J. Am. Chem. Soc.* **2000**, *122*, 7467−7479. (d) Lahav, M.; Heleg-Shabtai, V.; Wasserman, J.; Katz, E.; Willner, I.; Dürr, H.; Hu, Y.-Z.; Bossmann, S. H. *J. Am. Chem. Soc.* **2000**, *122*, 11480−11487.

(8) (a) Jang, S.-R.; Vittal, R.; Kim, K.-J. *Langmuir* **2004**, *20*, 9807−9810. (b) Lee, J. U. *Appl. Phys. Lett.* **2005**, *87*, 073101. (c) Landi, B. J.; Castro, S. L.; Ruf, H. J.; Evans, C. M.; Bailey, S. G.; Raffaelle, R. P. *Sol. Energy Mater. Sol. Cells* **2005**, *87*, 733−746. (d) Rud, J. A.; Lovell, L. S.; Senn, J. W.; Qiao, Q.; Mcleskey, J. T., Jr. *J. Mater. Sci.* **2005**, *40*, 1455−1458. (e) Kymakis, E.; Amaratunga, G. A. J. *Sol. Energy Mater. Sol. Cells* **2003**, *80*, 465−472. (f) Hasobe, T.; Fukuzumi, S.; Kamat, P. V. *Interface* **2006**, *15*, 47.

(9) (a) Fukuzumi, S.; Imahori, H. In *Electron Transfer in Chemistry*; Balzani, V., Ed.; Wiley−VCH: Weinheim, Germany, 2001; Vol. 2, pp 927−975. (b) Fukuzumi, S.; Guldi, D. M. In *Electron Transfer in* Chemistry; Balzani, V., Ed.; Wiley-VCH: Weinheim, Germany, 2001; Vol. 2, pp 270−337.

(10) (a) Imahori, H.; Tamaki, K.; Guldi, D. M.; Luo, C.; Fujitsuka, M.; Ito, O.; Sakata, Y.; Fukuzumi, S. *J. Am. Chem. Soc.* **2001**, *123*, 2607. (b) Imahori, H.; Guldi, D. M.; Tamaki, K.; Yoshida, Y.; Luo, C.; Sakata, Y.; Fukuzumi, S. *J. Am. Chem. Soc.* **2001**, *123*, 6617.

(11) (a) Imahori, H.; Hagiwara, K.; Akiyama, T.; Aoki, M.; Taniguchi, S.; Okada, T.; Shirakawa, M.; Sakata, Y. *Chem. Phys. Lett.* **1996**, *263*, 545. (b) Tkachenko, N. V.; Guenther, C.; Imahori, H.; Tamaki, K.; Sakata, Y.; Fukuzumi, S.; Lemmetyinen, H. *Chem. Phys. Lett.* **2000**, *326*, 344.

(12) (a) Imahori, H.; Yamada, H.; Guldi, D. M.; Endo, Y.; Shimomura, A.; Kundu, S.; Yamada, K.; Okada, T.; Sakata, Y.; Fukuzumi, S. *Angew. Chem., Int. Ed.* **2002**, *41*, 2344. (b) Imahori, H.; Tamaki, K.; Araki, Y.; Sekiguchi, Y.; Ito, O.; Sakata, Y.; Fukuzumi, S. *J. Am. Chem. Soc.* **2002**, *124*, 5165.

(13) Guldi, D. M.; Asmus, K.-D. *J. Am. Chem. Soc.* **1997**, *119*, 5744.

(14) Boyd, P. D. W.; Reed, C. A. *Acc. Chem. Res.* **2005**, *38*, 235.

(15) (a) Boyd, P. D. W.; Hodgson, M. C.; Rickard, C. E. F.; Oliver, A. G.; Chaker, L.; Brothers, P. J.; Bolskar, R. D.; Tham, F. S.; Reed, C. A. *J. Am. Chem. Soc.* **1999**, *121*, 10487. (b) Sun, D.; Tham, F. S.; Reed, C. A.; Chaker, L.; Burgess, M.; Boyd, P. D. W. *J. Am. Chem. Soc.* **2000**, *122*, 10704. (c) Sun, D.; Tham, F. S.; Reed, C. A.; Chaker, L.; Boyd, P. D. W. *J. Am. Chem. Soc.* **2002**, *124*, 6604. (d) Sun, D.; Tham, F. S.; Reed, C. A.; Boyd, P. D. W. *Proc. Natl. Acad. Sci. U.S.A.* **2002**, *99*, 5088.

(16) (a) Olmstead, M. M.; Costa, D. A.; Maitra, K.; Noll, B. C.; Phillips, S. L.; Van Calcar, P. M.; Balch, A. L. *J. Am. Chem. Soc.* **1999**, *121*, 7090. (b) Olmstead, M. M.; de Bettencourt-Dias, A.; Duchamp, J. C.; Stevenson, S.; Marciu, D.; Dorn, H. C.; Balch, A. L. *Angew. Chem., Int. Ed.* **2001**, *40*, 1223. (c) D'Souza, F.; Gadde, S.; Zandler, M. E.; Arkady, K.; El-Khouly, M. E.; Fujitsuka, M.; Ito, O. *J. Phys. Chem. A* **2002**, *106*, 12393.

(17) (a) Tashiro, K.; Aida, T.; Zheng, J.-Y.; Kinbara, K.; Saigo, K.; Sakamoto, S.; Yamaguchi, K. *J. Am. Chem. Soc.* **1999**, *121*, 9477. (b) Zheng, J.-Y.; Tashiro, K.; Hirabayashi, Y.; Kinbara, K.; Saigo, K.; Aida, T.; Sakamoto, S.; Yamaguchi, K. *Angew. Chem., Int. Ed.* **2001**, *40*, 1857.

(18) (a) Hasobe, T.; Kashiwagi, Y.; Absalom, M. A.; Sly, J.; Hosomizu, K.; Crossley, M. J.; Imahori, H.; Kamat, P. V.; Fukuzumi, S. *Adv. Mater.* **2004**, *16*, 975. (b) Hasobe, T.; Kamat, P. V.; Troiani, V.; Solladie, N.; Ahn, T. K.; Kim, S. K.; Kim, D.; Kongkanand, A.; Kuwabata, S.; Fukuzumi, S. *J. Phys. Chem. B.* **2005**, *109*, 19. (c) Hasobe, T.; Imahori, H.; Kamat, P. V.; Ahn, T. K.; Kim, S. K.; Kim, D.; Fujimoto, A.; Hirakawa, T.; Fukuzumi, S. *J. Am. Chem. Soc.* **2005**, *127*, 1216.

(19) Dai, H. J. *Acc. Chem. Res.* **2002**, *35*, 1035.

(20) Zhang, Y.; Iijima, S. *Phys. Rev. Lett.* **1999**, *82*, 3472.

(21) Freitag, M.; Perebeinos, V.; Chen, J.; Stein, A.; Tsang, J. C.; Misewich, J. A.; Martel, R.; Avouris, P. *Nano Lett.* **2004**, *4*, 1063.

(22) (a) O'Connell, M. J.; Bachilo, S. M.; Huffman, C. B.; Moore, V. C.; Strano, M. S.; Haroz, E. H.; Rialon, K. L.; Boul, P. J.; Noon, W. H.; Kittrell, C.; Ma, J. P.; Hauge, R. H.; Weisman, R. B.; Smalley, R. E. *Science* **2002**, *297*, 593. (b) Weisman, R. B.; Bachilo, S. M.; Tsyboulski, D. *Appl. Phys. A: Mater. Sci. Process.* **2004**, *78*, 1111. (c) Ma, Y. Z.; Stenger, J.; Zimmermann, J.; Bachilo, S. M.; Smalley, R. E.; Weisman, R. B.; Fleming, G. R. *J. Chem. Phys.* **2004**, *120*, 3368.

(23) Ando, T. *J. Phys. Soc. Jpn.* **1997**, *66*, 1066.

(24) (a) Barazzouk, S.; Hotchandani, S.; Vinodgopal, K.; Kamat, P. V. *J. Phys. Chem. B* **2004**, *108*, 17015. (b) Hasobe, T.; Fukuzumi, S.; Kamat, P. V. *Angew. Chem., Int. Ed.* **2006**, *45*, 755.

(25) (a) Okada, S.; Segawa, H. *J. Am. Chem. Soc.* **2003**, *125*, 2792. (b) Micali, N.; Mallamace, F.; Romeo, A.; Purrello, R.; Scolaro, L. M. *J. Phys. Chem. B* **2000**, *104*, 5897.

(26) (a) White, W. I. In *The Porphyrins*; Dolphin, D., Ed.; Academic Press: New York, 1979; Vol. V, Chapt. 7, pp 303−339. (b) Hambright, P. In *The Porphyrin Handbook*; Kadish, K. M., Smith, K. M., Guilard, R., Eds.; Academic Press: New York, 2000; Vol. 3, Chapt. 18, pp 129−210. (c) Katz, J. J.; Shipman, L. L.; Cotton, T. M.; Janson, T. R. In *The Porphyrins*; Dolphin, D., Ed.; Academic Press: New York, 1979; Vol. V, Chapt. 9, pp 401−458.

(27) (a) Ohno, O.; Kaizu, Y.; Kobayashi, H. *J. Chem. Phys.* **1993**, *99*, 4128. (b) Ribo, J. M.; Crusats, J.; Farrera, J.-A.; Valero, M. L. *J. Chem. Soc., Chem. Commun.* **1994**, 681. (c) Barber, D. C.; Freitag-Beeston, R. A.; Whitten, D. G. *J. Phys. Chem.* **1991**, *95*, 4074.

(28) (a) Pasternack, R. F.; Huber, P. R.; Boyd, P.; Engasser, G.; Francesconi, L.; Gibbs, E.; Fasella, P.; Venturo, G. C.; Hinds, L. de C. *J. Am. Chem. Soc.* **1972**, *94*, 4511. (b) Xu, W.; Guo, H.; Akins, D. L. *J. Phys. Chem. B.* **2001** *105*, 1543. (c) Castriciano, M. A.; Romeo, A.; Villari, V.; Micali, N.; Scolaro, L. M. *J. Phys. Chem. B.* **2003**, *107*, 8765. (d) Khairutdinov, R. F. *J. Phys. Chem. B* **1999**, *103*, 761.

(29) Amao, Y.; Komori, T. *Langmuir* **2003**, *19*, 8872.

(30) Hasobe, T.; Fukuzumi, S.; Kamat, P. V. *J. Am. Chem. Soc.* **2005**, *127*, 11884.

(31) Imahori, H.; Tamaki, K.; Araki, Y.; Sekiguchi, Y.; Ito, O.; Sakata, Y.; Fukuzumi, S. *J. Am. Chem. Soc.* **2002**, *124*, 5165.

(32) Chiang, I. W.; Brinson, B. E.; Huang, A. Y.; Willis, P. A.; Bronikowski, M. J.; Margrave, J. L.; Smalley, R. E.; Hauge, R. H. *J. Phys. Chem. B* **2001**, *105*, 8297.

(33) (a) Bedja, I.; Hotchandani, S.; Kamat, P. V. *J. Phys. Chem.* **1994**, *98*, 4133. (b) Girishkumar, G, Hall, T. D.; Vinodgopal, K.; Kamat, P. V. *J. Phys. Chem. B* **2006**, *110*, 107. (c) Kongakanad A.; Kuwabata, S.; Girishkumar, G.; Kamat, P. V. *Langmuir* **2006**, *21*, 2392.

(34) Hasobe, T.; Imahori, H.; Fukuzumi, S.; Kamat, P. V. *J. Mater. Chem.* **2003**, *13*, 2515.

(35) Rahman, G. M. A.; Guldi, D. M.; Campidelli, S.; Prato, M. *J. Mater. Chem.* **2006**, *16*, 62.

(36) (a) O'Connell, M. J.; Bachilo, S. M.; Huffman, C. B.; Moore, V. C.; Strano, M. S.; Haroz, E. H.; Rialon, K. L.; Boul, P. J.; Noon, W. H.; Kittrell, C.; Ma, J. P.; Hauge, R. H.; Weisman, R. B.; Smalley, R. E. *Science* **2002**, *297*, 593. (b) Weisman, R. B.; Bachilo, S. M.; Tsyboulski, D. *Appl. Phys. A: Mater. Sci. Process.* **2004**, *78*, 1111. (c) Ma, Y. Z.; Stenger, J.; Zimmermann, J.; Bachilo, S. M.; Smalley, R. E.; Weisman, R. B.; Fleming, G. R. *J. Chem. Phys.* **2004**, *120*, 3368. (d) Zhang, Y.; Iijima, S. *Phys. Rev. Lett.* **1999**, *82*, 3472.

(37) Kane, C. L.; Mele, E. J. *Phys. Rev. Lett.* **2003**, *90*, 207401.

(38) Pedersen, T. G. *Phys. Rev. B* **2003**, *67*, 073401.

(39) Spataru, C. D.; Ismail-Beigi, S.; Benedict, L. X.; Louie, S. G. *Phys. Rev. Lett.* **2004**, *92*, 017403.

(40) Fajer, J.; Davis, M. S. Electron Spin Resonance of Porphyrin Cations and Anions. In *The Porphyrins*; Dolphin, D., Ed.; Academic Press: New York, 1979; Vol. IV, pp 198−256.

(41) The intensity of dark current generation in OTE/SnO_2/SWCNT−H_4P^{2+} under an applied positive bias to the electrode is higher than that of our previous result of porphyrin−fullerene system. This may result from a strong interaction between SWCNT and I^-/I_3^- redox couple in the electrolyte system under no photoirradiation. See Supporting Information Figure S1 and the reference for the porphyrin−fullerene system: Hasobe, T. Imahori, H. Fukuzumi, S.; Kamat, P. V. *J. Phys. Chem. B* **2003**, *107*, 12105.

(42) The IPCE of OTE/SnO_2/SWCNT−H_4P^{2+} prepared from the suspension with high concentration of H_4P^{2+} (H_4P^{2+} 0.6 mM, SWCNT 1 mg) becomes smaller, probably because of too-high surface density of H_4P^{2+} on OTE/SnO_2/SWCNT−H_4P^{2+}. This in turn prevents the charge carrier transport in the thin film. Although the absorptivity becomes higher, the photoelectrochemical property becomes worse. See Supporting Information Figures S2 and S3.

(43) Power conversion efficiency of OTE/SnO_2/SWCNT−H_4P^{2+} is determined as 0.012%. See Supporting Information Figure S4.

(44) Robel, I.; Bunker, B. A.; Kamat, P. V. *Adv. Mater.* **2005**, *17*, 2458.

(45) (a) Ma, W.; Yang, C.; Gong, X.; Lee, K.; Heeger, A. J. *Adv. Funct. Mater.* **2005**, *15*, 1617, (b) Riedel, I.; von Hauff, E.; Parisi, J.; Martín, N.; Giacalone, F.; Dyakonov, V. *Adv. Funct. Mater.* **2005**, *15*, 1979, (c) Li, G.; Shrotriya, V.; Huang, J.; Yao, Y.; Moriarty, T.; Emery, K.; Yang, Y. *Nat. Mater.* **2005**, *4*, 864.